Scilight

Environmental Science and Geoscience
https://www.sciltp.com/journals/esg



Article

Promotive Effect of Ce Addition on Catalytic Oxidation of Vinyl Chloride over ZSM-5 Zeolite Supported Ru Catalysts

Xiang Zheng [1], Shuoming Wang [2], Maosheng Zhou [2] and Chuanhui Zhang [2,3,*]

[1] Faculty of Flavour Fragrance and Cosmetics, Shanghai Institute of Technology, Shanghai 201418, China
[2] Institute of Materials for Energy and Environment, College of Materials Science and Engineering, Qingdao University, Qingdao 266071, China
[3] Faculty of Chemical Engineering and Energy Technology, Shanghai Institute of Technology, Shanghai 201418, China
* Correspondence: zhangch@sit.edu.cn

How To Cite: Zheng, X.; Wang, S.; Zhou, M.; et al. Promotive Effect of Ce Addition on Catalytic Oxidation of Vinyl Chloride over ZSM-5 Zeolite Supported Ru Catalysts. *Environmental Science and Geoscience* **2026**, *1*(1), 5

Received: 14 September 2026
Revised: 21 October 2026
Accepted: 6 November 2026
Published: 16 November 2026

Abstract: Catalytic oxidation is an efficient end-of-pipe technology for eliminating toxic chlorinated volatile organic compounds (CVOCs) from industrial exhausts, yet developing high-performance zeolite supported Ru catalysts remains a hot topic in this field. Herein, a series of Ce-modified ZSM-5 zeolite supported RuO_x catalysts with gradient Ce loadings (0–7.5 wt.%) were fabricated via a two-step incipient wetness impregnation for vinyl chloride (VC) oxidation. Systematical characterizations demonstrate that appropriate Ce addition enriches oxygen vacancies and surface adsorbed oxygen, and greatly improves the low-temperature reducibility of Ru active sites. The 5%CeO_x-1%RuO_x/HZ5 catalyst exhibits the optimum catalytic activity, good cycling stability and stable activity retention in 20 h testing period with the lowest apparent activation energy. *In Situ* infrared spectroscopy reveals that Ce modification accelerates the oxidation of enol and carboxylate organic intermediates into CO_2 and H_2O. This work offers a fundamental understanding of Ce-promoted CVOCs removal over zeolite supported Ru catalysts.

Keywords: chlorinated volatile organic compounds; catalytic oxidation; cerium modification; ZSM 5 zeolite

1. Introduction

Chlorinated volatile organic compounds (CVOCs) are a class of highly toxic, refractory air pollutants widely released from industrial processes including plastic manufacturing, pesticide synthesis, waste incineration and polyvinyl chloride (PVC) production [1–3]. As a typical short-chain CVOCs, vinyl chloride (VC) monomer possesses strong carcinogenicity, low biodegradability and high atmospheric mobility. Uncontrolled emission of VC may cause severe damage to human respiratory and nervous systems while participating in photochemical smog and ozone layer destruction [4–6]. Among available end-of-pipe abatement technologies for CVOCs, catalytic oxidation stands out owing to its low operating temperature, high mineralization efficiency and low secondary pollution risk in comparison with thermal incineration, adsorption and biodegradation et al. [7–9]. Therefore, developing high-performance catalysts capable of completely decomposing VC into harmless CO_2, H_2O and HCl at moderate temperatures has become a research hotspot in environmental catalysis.

It has been previously demonstrated that supported ruthenium (Ru) catalysts are widely acknowledged as superior candidates for CVOC elimination owing to their remarkable capacity to cleave stable C–Cl and C=C bonds at low temperatures compared with those transition metal oxides [10–12]. Among variable support materials, MFI-type ZSM-5 zeolite has become a mainstream substrate for the dispersion of Ru active phases beneficially from its remarkable micro-porosity, large specific surface area, adjustable Brønsted/Lewis acid sites and adequate thermal stability [13–15]. The abundant acidic sites on H-type ZSM-5 (HZSM-5) zeolite can capture VC molecules and facilitate the dissociative dechlorination, while the pore confinement effect may

Copyright: © 2026 by the authors. This is an open access article under the terms and conditions of the Creative Commons Attribution (CC BY) license (https://creativecommons.org/licenses/by/4.0/).
Publisher's Note: Scilight stays neutral with regard to jurisdictional claims in published maps and institutional affiliations.

inhibit the agglomeration of Ru nanoparticles during high temperature calcination and reaction cycles [13,16]. Previous studies have verified that HZSM-5 supported Ru catalyst outperforms those Ru loaded on TiO_2, Al_2O_3 and CeO_2 supports in catalytic CVOCs oxidation, since the unique zeolite acid environment suppresses the generation of toxic polychlorinated byproducts from electrophilic chlorination of carbonaceous intermediates [17–20]. Nevertheless, the pristine HZSM-5 supported Ru catalysts still suffer from several intrinsic bottlenecks restricting their practical application. For examples, the weak metal-support interaction (MSI) between Ru and bare HZSM-5 zeolite may lead to an inferior low-temperature reducibility of Ru species, which requires higher reaction temperature for the initiation of VC oxidation simultaneously with larger apparent activation energy (E_a). In addition, the limited concentration of mobile surface adsorbed oxygen on the pristine HZSM-5 supported Ru catalyst may slow down the deep oxidation of organic intermediates, leaving chlorinated byproducts accumulation on catalyst surface. Moreover, the dissociated chlorine intermediates tend to occupy the Ru active sites and block the partial zeolite pores during long-term reaction period, consequently inducing gradual decline of catalytic activity and durability. To address these drawbacks, many researchers have explored multiple modification strategies towards ZSM-5 supported Ru catalyst, such as constructing hierarchical pores via alkali etching, doping transition metals (Cu, Mn and Co) and adjusting Si/Al ratios [17,21–24], yet these approaches often bring new trade-offs, such as zeolite crystallinity damages by excessive alkali treatment, and the sacrifice of surface acid sites or the risk aggravation of chlorine poisoning after transition metal doping.

Rare earth ceria oxide (CeO_2) has emerged as an ideal functional modifier for Ru-based CVOCs catalysts due to its reversible Ce^{3+}/Ce^{4+} redox cycle and abundant intrinsic oxygen vacancies [25,26]. The valence transformation between Ce^{3+} and Ce^{4+} continuously generates surface oxygen vacancies, which greatly accelerate the adsorption and activation of gaseous oxygen molecules to form highly reactive surface adsorbed oxygen (O_{ads}), which are the dominant active species responsible for breaking C=C and C-Cl bonds [27,28]. More importantly, the intimate contact between CeO_2 and RuO_x could trigger strong electronic interaction, which regulates the valence distribution of Ru, lowers the reduction temperature of Ru oxides and simultaneously optimizes the dispersion of Ru nanoparticles on zeolite surfaces [29]. It has been previously confirmed that Ce doping effectively reduced the E_a of CVOCs oxidation and improves the catalytic cycling stability [30–32]. However, most existing studies directly employ pure CeO_2 as the pristine support rather than modifying additive for zeolites supported Ru catalysts. In addition, there are few investigations systematically discussing the quantitative correlation between surface deposition of Ce and the textural, acidity, redox properties as well as catalytic activities over zeolite supported Ru catalysts.

In this work, a series of Ce-modified HZSM-5 supported RuO_x catalysts with gradient Ce loadings (0–7.5 wt.%) were fabricated via a two-step incipient wetness impregnation. Comprehensive characterization techniques, catalytic and kinetics experiments were applied to systematically explore the structure-activity relationship and the modification role of Ce addition in catalytic VC oxidation. Furthermore, *in situ* diffuse reflectance infrared Fourier transform spectroscopy (DRIFTs) analysis was performed to capture the real-time VC adsorption behaviours and possible organic intermediates in order to unravel the intrinsic catalytic pathways over the prepared catalysts.

2. Experimental

2.1. Catalyst Preparation

The ZSM-5 zeolite with a Si/Al ratio of 50 was prepared by a hydrothermal method, and the synthesis details are described in the Supplementary Material. HZSM-5 zeolite supported RuO_x catalysts with variable amounts of Ce addition was prepared by using a two-step incipient wetness impregnation method. To be precise, the HZSM-5 zeolite support was added to certain amount of cerium nitrate aqueous solution with variable cerium loadings (2.5 wt.%, 5 wt.%, or 7.5 wt.% of Ce on ZSM-5 support), respectively. After static aging at room temperature for 4 h, the material was dried overnight at 80 °C and calcined in a muffle furnace at 400 °C for 4 h. Subsequently, a certain volume of $RuCl_3$ aqueous solution (0.02 g_{Ru} mL^{-1}) was dropped onto the Ce-modified HZSM-5 zeolite support. After static aging at room temperature for 4 h, the solid material was dried overnight at 80 °C and calcined again in air at 400 °C for 4 h. It should be clearly pointed out that the nominal loading of Ru in the catalyst was 1 wt.% with regard to the zeolite support. For simple description below, the prepared catalysts were denoted as 2.5%CeO_x-1%RuO_x/HZ5, 5%CeO_x-1%RuO_x/HZ5 and 7.5%CeO_x-1%RuO_x/HZ5 on the basis of the content of Ce. The catalyst without any Ce addition was designated as 1%RuO_x/HZ5.

2.2. Catalyst Characterizations

The prepared catalysts were characterized by several techniques including X-ray diffraction (XRD), scanning electron microscope (SEM), transmission electron microscope (TEM), physical and chemical sorption, and X-ray photoelectron spectroscopy (XPS). The reaction mechanism and intermediates were studied by *in situ* diffuse DRIFTs. More details are provided in the Supplementary Material.

2.3. Catalytic Testing

Catalytic reaction of VC oxidation was conducted in a typical tubular fixed-bed reactor under atmospheric pressure. For catalytic activity evaluation, 200 mg of catalyst particles (40–60 mesh) was deposited in the middle position of the reactor, and the reactant feed with a total flow rate of 50 mL min^{-1} was composed by 0.1 vol.% VC, 8.0 vol.% O_2 and the residual Ar as the balance, giving a weight hourly space velocity (WHSV) of 15,000 mL g^{-1} h^{-1}. VC adsorption-desorption equilibrium was achieved after a static maintenance of the reactor at 100 °C for 1 h, following by the temperature-programmed operation from 100 to 350 °C with a plateau at each testing temperature point for 0.5 h prior to sampling analysis. VC and possible organics in catalytic reaction was analysed by an online gas chromatograph (Fuli 9790, Taizhou, China) with a flame ionization detector (FID), and VC conversion was determined on the basis of concentration difference in the inlet and outlet, respectively. Regarding the catalytic measurement reproducibility, all catalytic experiments were repeated over two independent catalyst batches for each sample. Each batch was subjected to at least one full temperature-programmed VC oxidation run.

3. Results and Discussion

3.1. Crystalline Phase

Figure 1 shows the XRD patterns of the prepared 1%RuO_x/HZ5 and y%CeO_x-1%RuO_x/HZ5 (y = 2.5, 5, 7.5) catalysts. By referencing ICDD PDF database, typical characteristic diffraction peaks assignable to MFI-type ZSM-5 zeolites can be observed in the 2θ angle ranges of 7–9°, 22–25°, and 44.5–46° for all prepared catalysts [33]. Notably, the diffraction peaks intensity gradually decreases with the increasing content of Ce over the Ce-modified catalysts. In addition, 2.5%CeO_x-1%RuO_x/HZ5 exhibits relatively higher crystallinity comparable to 1%RuO_x/HZ5, which indicates that an appropriate amount of Ce addition is favourable to the crystallinity enhancement of the catalyst. Meanwhile, no characteristic diffraction peaks corresponding to RuO_x are detectable in the XRD patterns of all catalysts, which may be attributed to the good surface dispersion or low loading of Ru species. In contrast, one can note the distinct appearance of characteristic peaks attributable to CeO_2 in the 2θ ranges of 28–29° and 47–49° over the Ce-modified RuO_x/HZ5 catalysts, which implies the surface enrichment of Ce species primarily in the form of CeO_2 on the catalyst surface.

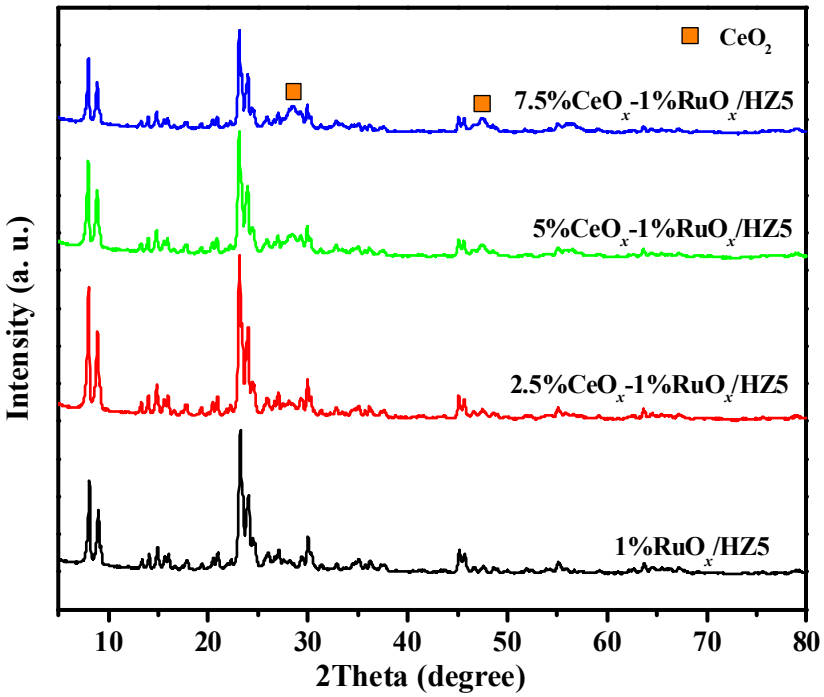

Figure 1. XRD patterns of all prepared catalysts.

3.2. Surface Morphology and Micro-Structure

SEM images of the prepared catalysts are shown in Figure 2. Notably, each catalyst exhibits similar cylindrical morphology with cross-sectional dimensions of approximately 200 nm. Furthermore, the prepared catalysts demonstrate relatively smooth surface and well-defined nanoparticles, which indicates that the addition of Ce doesn't alter the morphological feature of the HZSM5 zeolite supported RuO_x catalysts.

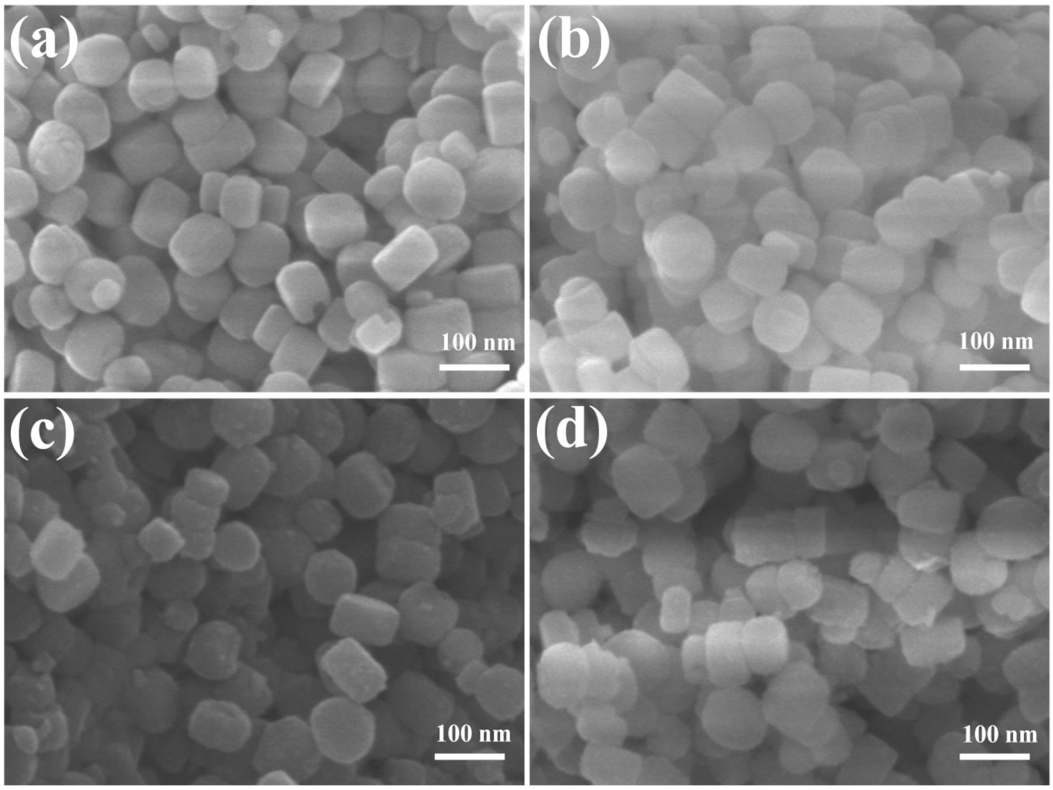

Figure 2. SEM images of (**a**) 1%RuO_x/HZ5, (**b**) 2.5%CeO_x-1%RuO_x/HZ5, (**c**) 5%CeO_x-1%RuO_x/HZ5, (**d**) 7.5%CeO_x-1%RuO_x/HZ5.

TEM images in Figure 3 reveals that there is no significant difference in the basic morphology and crystalline size between the Ce-modified RuO_x/HZ5 (Figure 3c,e,g) and the pristine 1%RuO_x/HZ5 (Figure 3a) catalysts. This observation confirms that the addition of Ce doesn't alter the original morphological structure of 1%RuO_x/HZ5 catalyst. Meanwhile, it is worth noting that there appears more obvious dispersion of cerium oxide nanoparticles on the catalyst surface with the increasing addition of Ce, which indicates the surface presence and enrichment of Ce species on the ZSM-5 zeolite. Additionally, one can find the sign about mesopores formation over all prepared catalysts, which may be attributed to the excessive TPAOH template during ZSM-5 synthesis. The infiltration of OH^- ions into the zeolite framework likely results in the partial corrosion of silica species, thus leading to the formation of some mesopores in ZSM-5 crystals [13,34]. High-resolution TEM (HR-TEM) images in Figure 3b,d,f,h further reveals the distinct lattice fringes with the interplanar spacings of 0.312 and 0.256 nm, characteristically assignable to the (111) facet of CeO_2 and (101) facet of RuO_2, respectively [35,36]. These results demonstrate the successful formation of CeO_2 and RuO_2 crystalline phases onto the ZSM-5 support via impregnation methods.

The nitrogen adsorption-desorption isotherms and pore-size distributions of the prepared catalysts are shown in Figure 4. As seen in Figure 4a, all catalysts exhibit Type I isotherm characteristics, which indicates their dominant microporous framework. Specifically, the adsorption behaviour at the low relative pressure range of $p/p_0 < 0.1$ confirms the presence of micropores in the catalysts. In the medium relative pressure region ($0.3 < p/p_0 < 0.8$) and high relative pressure region ($p/p_0 > 0.8$), one can note the appearance of H4-type hysteresis loops, which reflects the construction of a hierarchical porosity consisting of micropores and mesopores [16,22]. This finding is well consistent with the TEM images, which both reveals the successful formation of hierarchical architecture. As depicted in Figure 4b, the pore-size distribution further confirms the hierarchical porous structure of the catalysts with the pore-size predominantly cantered at ca. 2 and 4 nm. However, the Ce-modified catalysts show no significant difference in the pore-size distribution in comparison with the pristine 1%RuO_x/HZ5 catalyst. On the basis of the specific surface area (SSA) data in Table 1, one can find that the SSA gradually decreases with the increasing addition of Ce into the catalysts from 1%RuO_x/HZ5 to 7.5%CeO_x-1%RuO_x/HZ5. This phenomenon can be explained that the more loading of Ce species on the catalyst would induce a block effect on the existing pores.

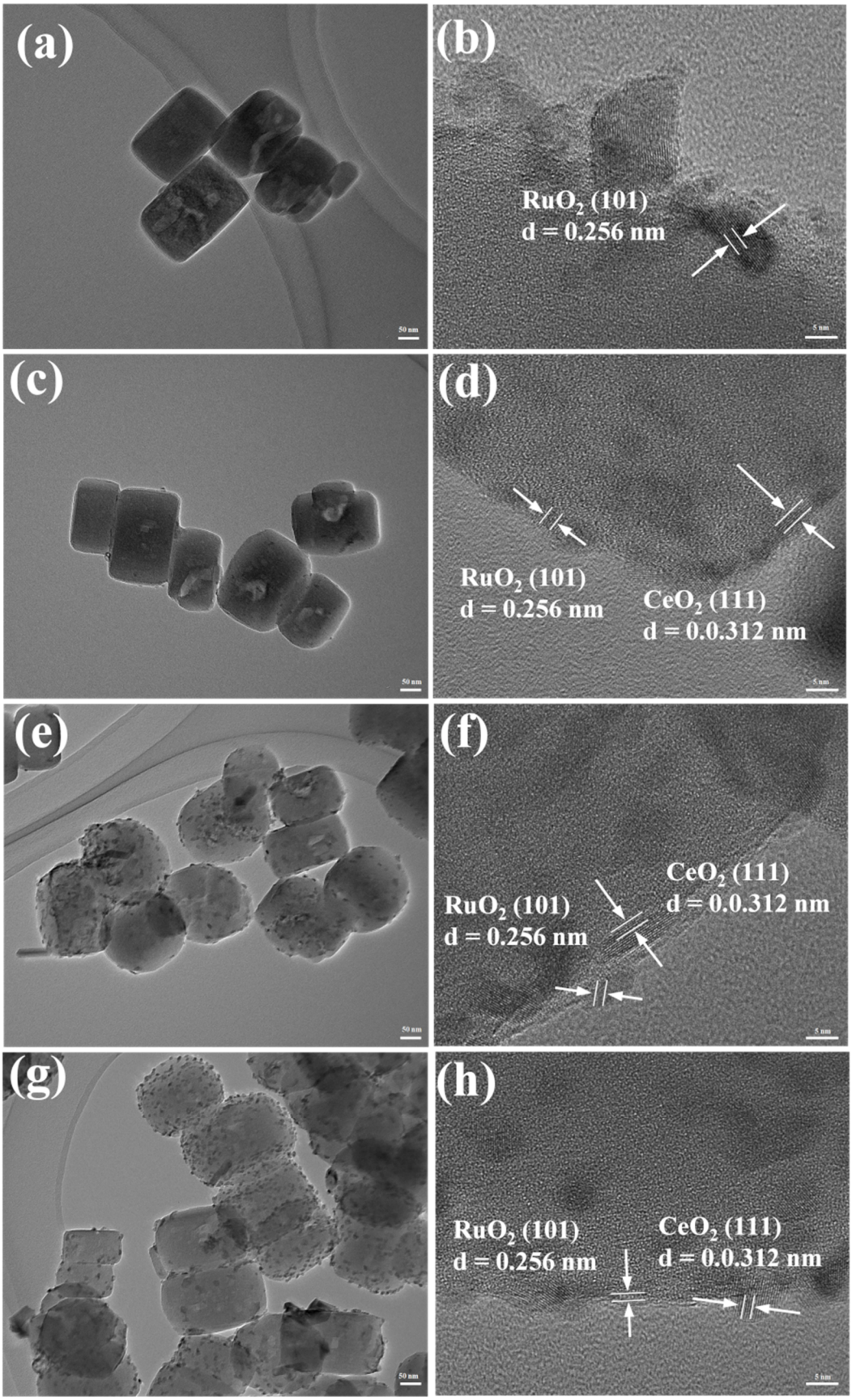

Figure 3. TEM images of (**a**,**b**) 1%RuO_x/HZ5, (**c**,**d**) 2.5%CeO_x-1%RuO_x/HZ5, (**e**,**f**) 5%CeO_x-1%RuO_x/HZ5, and (**g**,**h**) 7.5%CeO_x-1%RuO_x/HZ5.

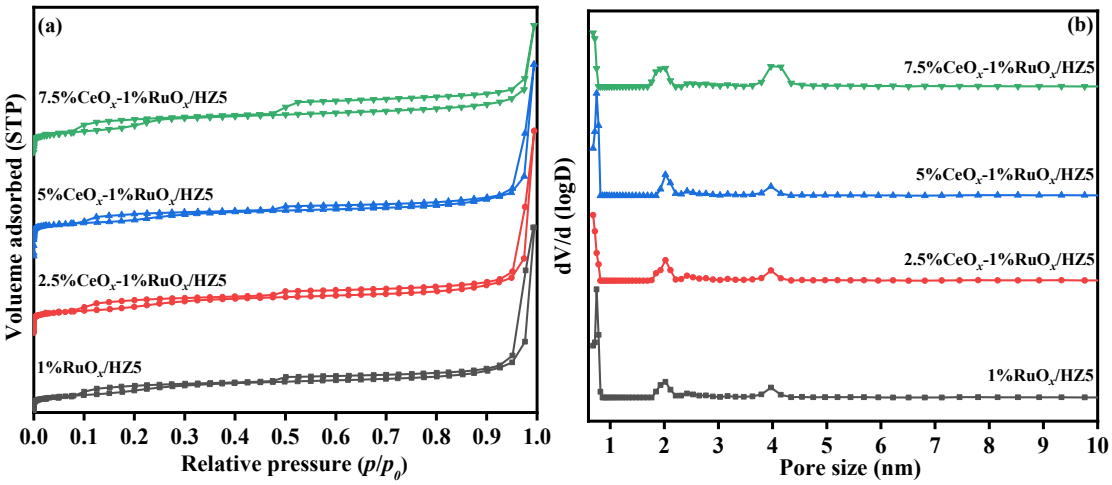

Figure 4. (**a**) Nitrogen adsorption-desorption isotherms and (**b**) pore-size distributions of the prepared catalysts.

Table 1. Porosity properties of all prepared catalysts.

Catalysts	SSA [a]	Mesopore Volume [b]	Toal Pore Volume [a]
	$m^2\ g^{-1}$	$cm^3\ g^{-1}$	$cm^3\ g^{-1}$
1%RuO_x/HZ5	374	0.475	0.626
2.5%CeO_x-1%RuO_x/HZ5	371	0.504	0.658
5%CeO_x-1%RuO_x/HZ5	360	0.446	0.594
7.5%CeO_x-1%RuO_x/HZ5	323	0.303	0.603

[a] Determined by BET method; [b] Determined by BJH method (adsorption branch).

3.3. Reducibility and Surface Acidity

Figure 5 presents the H_2-TPR profiles of the prepared catalysts. All catalysts exhibit low-temperature reduction peaks without obvious high-temperature reduction signal, which indicates the weak interaction between the active RuO_x and the ZSM-5 zeolite support. Notably, the Ce-modified catalysts demonstrate relatively lower reduction temperature comparable to the pristine 1%RuO_x/HZ5, which reflects the low-temperature reducibility enhancement by Ce modification. Among all, 5%CeO_x-1%RuO_x/HZ5 exhibits not only the lowest reduction temperature but also the weakest reduction signal intensity. This phenomenon implies that a proper content of Ce addition can facilitate the reducible behaviour of surface RuO_x.

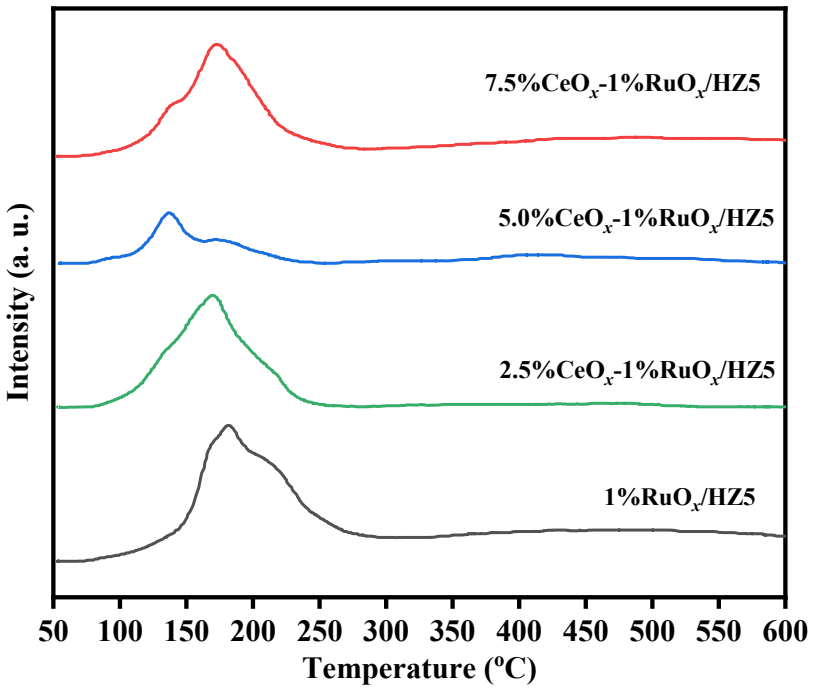

Figure 5. H_2-TPR profiles of all prepared catalysts.

The surface acidity of the prepared catalysts was analysed by NH_3-TPD experiments, and the recorded profiles are shown in Figure 6. One can find that the desorption peak cantered at 100 °C primarily arises from the physical adsorption of ammonia on the acid sites of ZSM-5 zeolite (denoted as Peak 1). With the temperature rise, the noticeable appearance of desorption signal in the range of 245–500 °C can be generally original from the chemical adsorption of ammonia on the acid sites of the catalyst. The desorption peaks in the temperature regions of 250–400 and 400–500 °C are denoted as Peak 2 and Peak 3, respectively. It is worth noting that the 7.5%CeO_x-1%RuO_x/HZ5 catalyst exhibits relatively lower desorption peak intensity in the region of Peak 1 in comparison with the other catalysts. This phenomenon can be explained that excessive Ce addition would result in the pore blockage on the catalyst, thereby reducing the exposure of surface acid sites. Additionally, each catalyst presents several desorption peaks above 400 °C, which indicates the presence of strong acid sites. Among all, 5%CeO_x-1%RuO_x/HZ5 exhibits higher desorption temperature in the high-temperature region, which suggests its stronger surface acidity that would be favourable to the catalytic oxidation of VC. According to the quantitative results in Table 2, 2.5%CeO_x-1%RuO_x/HZ5 and 7.5%CeO_x-1%RuO_x/HZ5 catalysts exhibit lower peak areas than the pristine 1%RuO_x/HZ5, while the 5%CeO_x-1%RuO_x/HZ5 catalyst demonstrates a significantly larger peak area corresponding to strong acid sites at 443 °C, suggesting its outstanding surface acidity property.

Table 2. Quantitative results of XPS and NH_3-TPD analysis over the prepared catalysts.

Catalysts	O_{ads}/O_{total} [a]	Ce^{3+}/Ce^{4+} [a]	Area Integration of Desorption Peak [b]			
			Peak 1	Peak 2	Peak 3	Total
1%RuO_x/HZ5	0.56	-	229	476	-	705
2.5%CeO_x-1%RuO_x/HZ5	0.67	0.43	224	174	-	398
5%CeO_x-1%RuO_x/HZ5	0.69	0.48	310	226	313	849
7.5%CeO_x-1%RuO_x/HZ5	0.68	0.38	197	245	253	695

[a] Determined from XPS spectra; [b] Determined from NH_3-TPD profiles.

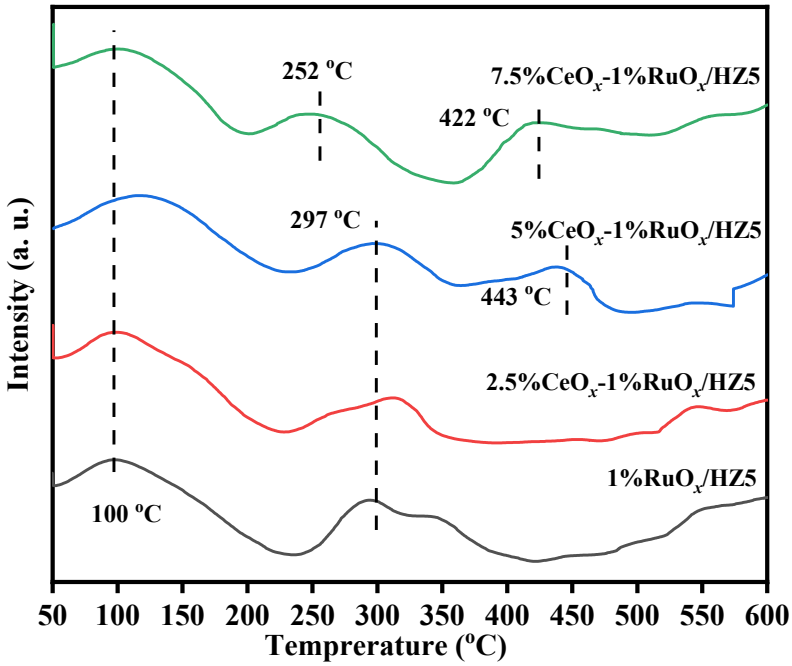

Figure 6. NH_3-TPD profiles of all prepared catalysts.

3.4. Surface Elemental Analysis

XPS analysis was conducted in order to investigate the surface elemental composition and chemical states on the catalysts, and the characteristic XPS spectra of Ru 3d, Al 2p, Si 2p and O 1s are shown in Figure 7. Figure 7a presents the survey spectra of all catalyst, illustrating the elemental compositions on the catalyst surface. As seen in Figure 7b, the XPS spectra of Ru 3d + C 1s are primarily deconvoluted into two spin-orbit components namely as Ru $3d_{5/2}$ at 280.7 eV and Ru $3d_{3/2}$ at 285.7 eV assignable to Ru^{4+} cations, which indicates the predominant formation of RuO_2 crystalline phases on the catalyst surface [37,38]. Additionally, the deconvoluted peaks at 284.6 and 288.6 eV for C 1s spectra are attributed to the signal of C-C and C=O bonds, respectively, which may be associated with adsorbed organic contaminants on the catalyst surface or residual organic templates in the zeolite synthesis process [15,39].

The Ce 3d spectra of the Ce-modified catalysts are shown in Figure 7c. The Ce 3d spectra are deconvoluted into two spin-orbit counterparts of Ce $3d_{3/2}$ and Ce $3d_{5/2}$. The XPS peaks at the binding energies (BE) of 901.4 (u), 903.4 (u′), 907.4 (u″) and 917.0 (u‴) eV are assigned to the Ce $3d_{3/2}$ orbit, while those at 882.7 (v), 884.8 (v′), 889.4 (v″) and 898.7 (v‴) eV correspond to the Ce $3d_{5/2}$ orbital [40,41]. Peak deconvolution analysis indicates that the signal at 884.8 (v′) and 903.4 (u′) eV are attributed to Ce^{3+} cations, whereas the remaining peaks primarily represent Ce^{4+} cations [42,43]. The coexistence of Ce^{3+} and Ce^{4+} cations in the catalyst may arise from the presence of oxygen vacancies or lattice defects within CeO_2, thus inducing valence state transitions of Ce^{4+}. Furthermore, the surface Ce^{3+}/Ce^{4+} redox couples can promote the adsorption of surface oxygen species and thereby boost the catalytic oxidation activity. As listed in Table 2, the 5%CeO_x-1%RuO_x/HZ5 catalyst possesses the highest molar ratio of Ce^{3+}/Ce^{4+}, which signifies its potentiality of higher catalytic activity in the reaction.

The Al and Si species in the prepared catalysts primarily contribute to the framework construction of ZSM-5 zeolite support, and one can find that the addition of Ce doesn't significantly affect the surface Al and Si species in the catalyst in Figure 7d,e. It means that Ce modification doesn't alter the framework structure of ZSM-5 zeolite, which is consistent with the microscopic morphology of the catalysts. As seen from Figure 7f, the O 1s spectra can be deconvoluted into three peaks at BE of 529.4, 532.6, and 533.4 eV, which are typically attributable to lattice oxygen (O_{latt}), surface adsorbed oxygen (O_{ads}), and surface adsorbed water or hydroxyl species, respectively [7,16,27]. Generally, O_{ads} species are considered to be more active than O_{latt} due to their superior mobility and lower surface bonding energy. The quantitative results of O_{ads}/O_{total} molar ratio in Table 2 reveal that Ce-modified catalysts exhibit a relatively higher molar ratio of O_{ads}/O_{total} in comparison with the pristine 1%RuO_x/HZ5 catalyst, which indicates that Ce modification is favourable to the adsorption of surface oxygen species on the catalyst. Amongst, the 5%CeO_x-1%RuO_x/HZ5 catalyst possesses the highest molar ratio of O_{ads}/O_{total}, which reflects the most plentiful surface oxygen species from the optimum addition of Ce.

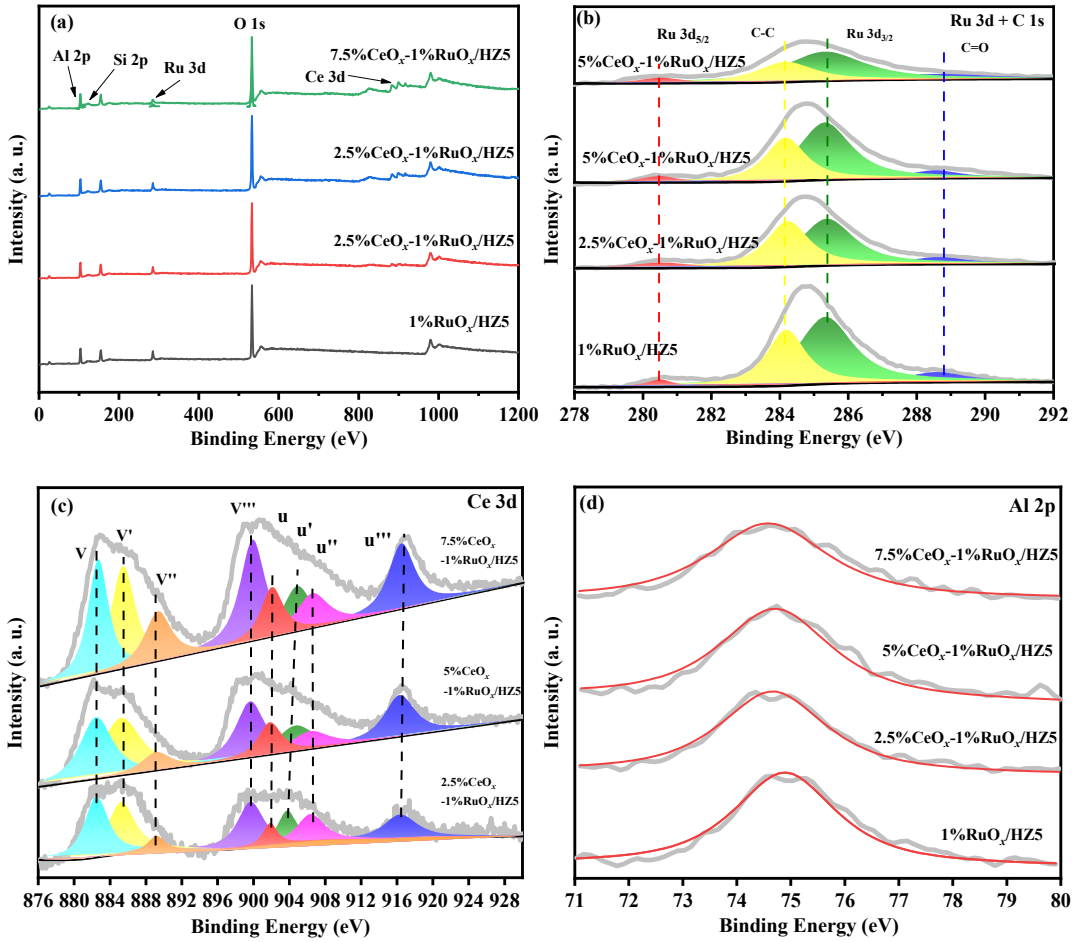

Figure 7. *Cont.*

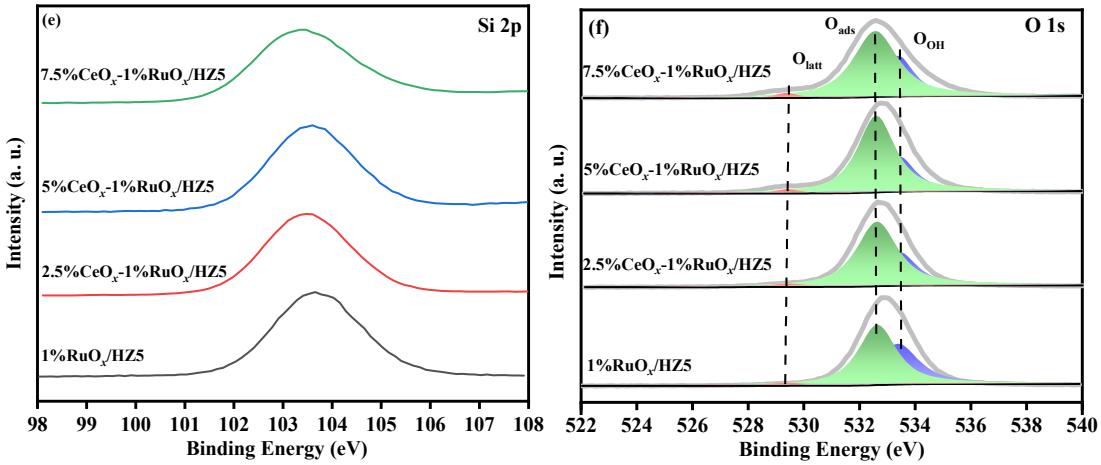

Figure 7. (**a**) XPS full spectra and XPS spectra of (**b**) Ru 3d, (**c**) Ce 3d, (**d**) Al 2p, (**e**) Si 2p and (**f**) O 1s over the prepared catalysts.

3.5. Catalytic Performance for VC Oxidation

The catalytic performances of the prepared catalyst for VC oxidation were evaluated through the measurements of catalytic activity, long-term stability and kinetics, and the obtained results are shown in Figure 8. As depicted in Figure 8a, the Ce-modified catalysts exhibit higher catalytic activity compared to 1%RuO_x/HZ5 in the temperature range of 50–350 °C. With regards to the light-off curves in Figure 8a and the representative temperatures at 50% and 90% conversion (denoted as T_{50} and T_{90}) in Table 3, the catalytic activities for VC oxidation over the catalysts follow the decreasing order of 5%CeO_x-1%RuO_x/HZ5 > 2.5%CeO_x-1%RuO_x/HZ5 > 7.5%CeO_x-1%RuO_x/HZ5 > 1%RuO_x/HZ5. Notably, 5%CeO_x-1%RuO_x/HZ5 gives the T_{50} and T_{90} values of 270 and 290 °C, which are 27 and 31 °C lower than those of the pristine 1%RuO_x/HZ5. Even for 7.5%CeO_x-1%RuO_x/HZ5, its T_{50} and T_{90} are still 20 °C lower than those of 1%RuO_x/HZ5. Based on these results, it can be concluded that the addition of Ce into 1%RuO_x/HZ5 catalyst can significantly boost its catalytic activity for VC oxidation, which is reasonably attributed to the abundant surface adsorbed oxygen species and the higher low-temperature reducibility. Considering the presence of HCl and Cl_2 in the effluent would cause severe corrosion to the thermal conductivity detector and methanizer, the selectivity of CO_2 was not measured, thus carbon and chlorine balances could not be obtained. Moreover, minor chlorinated organic byproducts, namely dichloromethane (CH_2Cl_2), chloroform ($CHCl_3$), carbon tetrachloride (CCl_4), and 1,1,2-trichloroethane ($CH_2ClCHCl_2$), emerged within the temperature window of 200–300 °C. These chlorinated byproducts existed at trace ppm concentrations, with a maximum value of 50 ppm, which was consistent with their very weak chromatographic signals. This observation reflects the high capacity of the as-prepared catalysts for VC mineralization.

The catalytic stability of 5%CeO_x-1%RuO_x/HZ5 for VC oxidation were examined in multiple catalytic runs. As shown in Figure 8b, the light-off curves in three catalytic runs are nearly overlapped, which strongly demonstrates the excellent catalytic stability of 5%CeO_x-1%RuO_x/HZ5 in the reaction. Meanwhile, the catalytic durability tests were also conducted over 5%CeO_x-1%RuO_x/HZ5. In Figure 8c, one can note that the catalyst maintains VC conversion of 50 and 90% at 270 and 290 °C during the testing period of 20 h, which indicates its stable activity retention. In order to make better comparison about the low-temperature catalytic activity of these catalysts, the apparent activation energy (E_a) for catalytic VC oxidation was calculated by Arrhenius equation under strict kinetic conditions (VC conversion controlled below 15%). On the basis of the linear Arrhenius plots in Figure 8d and the E_a values in Table 3, it can be observed that E_a for the prepared catalyst follows a descending sequence of 1%RuO_x/HZ5 (105 kJ mol^{-1}) > 7.5%CeO_x-1%RuO_x/HZ5 (84 kJ mol^{-1}) > 2.5%CeO_x-1%RuO_x/HZ5 (74 kJ mol^{-1}) > 5%CeO_x-1%RuO_x/HZ5 (61 kJ mol^{-1}). This sequence closely aligns with their catalytic activity order for VC oxidation. Compared to the pristine 1%RuO_x/HZ5, the Ce-modified catalysts exhibit lower E_a values, which indicates that Ce modification significantly enhances the activation capacity of active Ru components towards VC molecules on the catalyst.

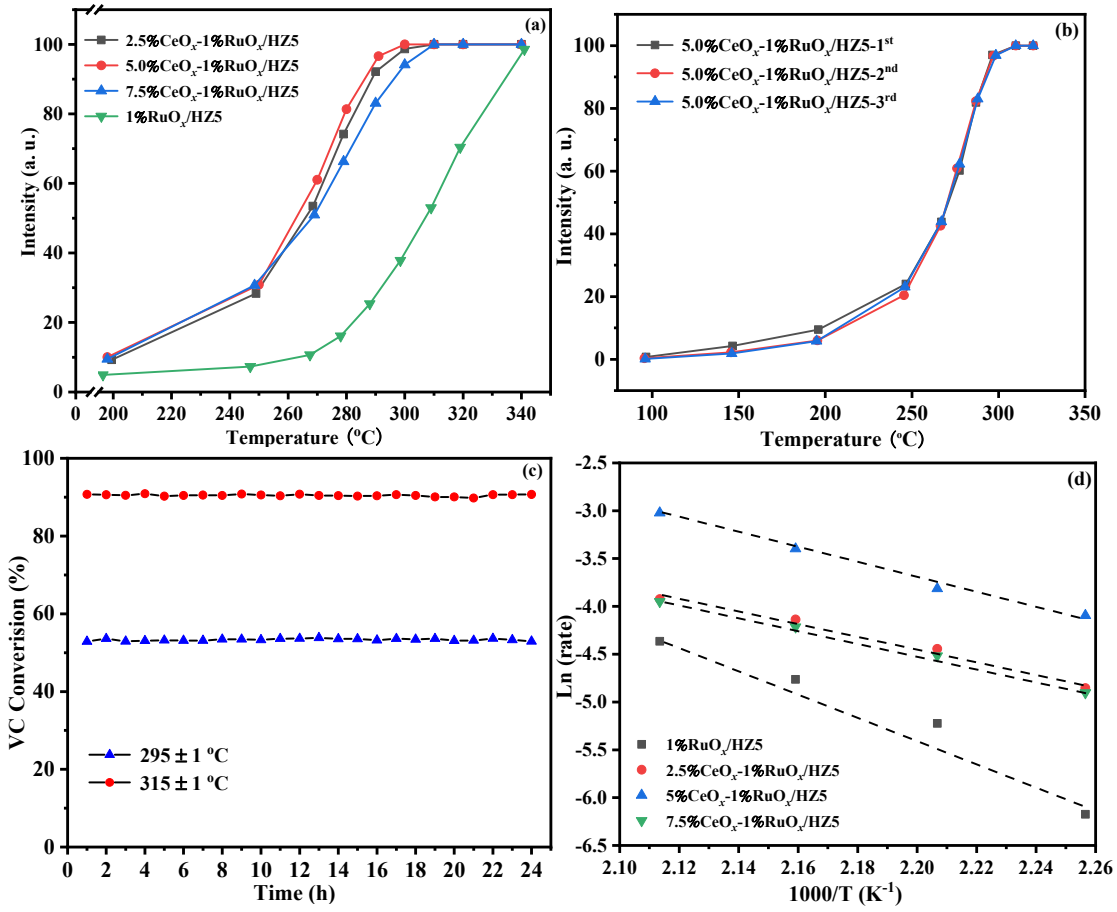

Figure 8. (**a**) Light-off curves of VC conversion versus reaction temperature over all prepared catalysts, (**b**) Catalytic stability test over 5%CeO_x-1%RuO_x/HZ5 in multiple catalytic runs, (**c**) Long-term catalytic durability test over 5%CeO_x-1%RuO_x/HZ5 at T_{50} and T_{90}, and (**d**) Arrhenius plots.

Table 3. Representative parameters for catalytic performance comparison over the prepared catalysts.

Catalysts	Representative Temperature (°C)		E_a (kJ mol^{-1})
	T_{50}	T_{90}	
1%RuO_x/HZ5	297 ± 2	321 ± 3	105 ± 3
2.5%CeO_x-1%RuO_x/HZ5	275 ± 3	295 ± 3	74 ± 2
5%CeO_x-1%RuO_x/HZ5	270 ± 2	290 ± 3	61 ± 3
7.5%CeO_x-1%RuO_x/HZ5	275 ± 3	298 ± 3	84 ± 2

3.6. Catalytic Mechanism

In Situ DRIFTs experiments were conducted over the 5%CeO_x-1%RuO_x/HZ5 and 1%RuO_x/HZ5 catalysts under inert and oxygen atmospheres at room temperature and variable temperatures, which aims to study the surface adsorption-transformation behaviours of VC molecules and the possible formation of organic intermediates. Figure 9a,b presents the IR spectra of VC adsorption on 1%RuO_x/HZ5 and 5%CeO_x-1%RuO_x/HZ5 at 50 °C within different time intervals. One can find that the intensity of IR peaks at 711, 1324 and 1605 cm^{-1} gradually increases with the prolonged time until stabilization. These peaks are attributed to the vibrations of C-Cl, C-H, and C=C bonds in VC molecule, respectively, which indicates that more VC molecules are adsorbed on the catalyst surface with the time extension [44–46]. Meanwhile, it can be observed that 5%CeO_x-1%RuO_x/HZ5 requires 8 min to reach VC adsorption equilibrium at 50 °C, which is longer than 1%RuO_x/HZ5. This phenomenon may be due to the loading of cerium oxide on the catalyst surface, thus partially covering the pores and slowing down the adsorption process. Additionally, the characteristic IR signal of enol species appears around 1205 cm^{-1} with gradual increasing intensity over time [46,47]. These species are typically regarded as the organic intermediates in catalytic VC oxidation. This observation suggests that the presence of surface adsorbed oxygen species can facilitate the oxidative activation and conversion of VC molecules even under an inert and room temperature condition.

Figure 9c,d shows the *in situ* DRIFTs results of 1%RuO_x/HZ5 and 5%CeO_x-1%RuO_x/HZ5 under an inert atmosphere. The characteristic peaks at approximately 718, 1315, and 1582 cm^{-1} correspond to the C-Cl, C-H, and

C=C bonds of VC molecules, respectively, and their intensities gradually decreased with increasing temperature [46,47]. Meanwhile, the characteristic peaks around 2350 represent CO_2, with their intensities gradually increasing as the temperature rises [16,48]. Notably, the 5%CeO_x-1%RuO_x/HZ5 catalyst exhibits a higher peak intensity around 2358 cm^{-1}, indicating that the catalyst can effectively catalyse the conversion of VC into CO_2 and H_2O as the temperature increases. This phenomenon is attributed to the enhanced activation capability of adsorbed active oxygen species on the catalyst surface at elevated temperatures, which promotes the catalytic oxidation of VC. Additionally, intermediate species were observed during the conversion of VC. The characteristic peak around 1202 cm^{-1} corresponds to enol-like species, while the peak around 1706 cm^{-1} represents carboxylate species [46,48]. The characteristic peak of enol-like species around 1202 cm^{-1} disappears with the rise of temperature, which not only suggests the formation of intermediate species during the catalytic oxidation of VC but also indicates that surface active oxygen species at high temperatures can facilitate the conversion of these intermediates.

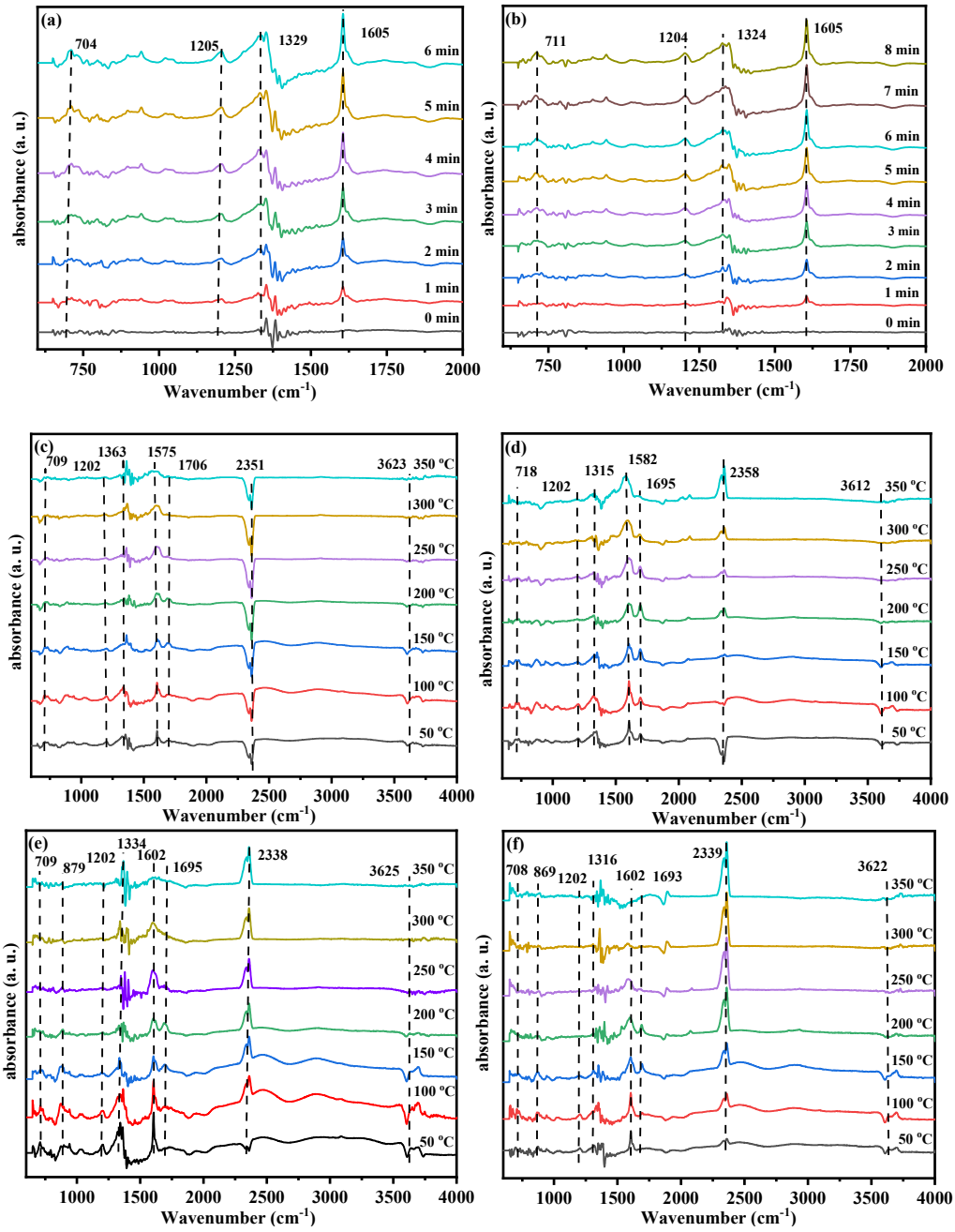

Figure 9. *In Situ* DRIFTs results of VC adsorption at 50 °C at different time over (**a**) 1%RuO_x/HZ5 and (**b**) 5%CeO_x-1%RuO_x/HZ5, *in situ* DRIFTs results of catalytic VC oxidation in the absence of gas phase oxygen over (**c**) 1%RuO_x/HZ5 and (**d**) 5%CeO_x-1%RuO_x/HZ5, *in situ* DRIFTs results of catalytic VC oxidation in the presence of gas phase oxygen over (**e**) 1%RuO_x/HZ5 and (**f**) 5%CeO_x-1%RuO_x/HZ5.

Figure 9e,f illustrates the *in situ* DRIFTs results of catalytic VC oxidation over 1%RuO_x/HZ5 and 5%CeO_x-1%RuO_x/HZ5 catalysts under an oxygen atmosphere. Compared with the IR spectra in Figure 9c,d under an inert condition, the characteristic IR bands assignable to CO_2 and H_2O at ca. 2350 and 2620 cm^{-1} display much higher intensities, revealing that the catalytic activity is greatly boosted with the participation of gaseous oxygen and thereby promotes the oxidation of VC into more CO_2 and H_2O. Meanwhile, the intensities of IR bands at ca. 709, 1334 and 1602 cm^{-1} corresponding to C–Cl, C–H and C=C gradually decline as the temperature rises. This observation indicates that the efficient catalytic conversion of VC under an oxygen atmosphere drastically reduces the accumulation of adsorbed VC on the catalyst surface. In comparison with 1%RuO_x/HZ5, 5%CeO_x-1%RuO_x/HZ5 exhibits relatively weaker intensities of IR bands attributable to enol and carboxylate intermediates at ca. 1202 and 1693 cm^{-1} at the same temperature, which demonstrates that this catalyst accelerates the rapid oxidation of organic intermediates. Such superiority originates from the Ce modification effect upon the parent 1%RuO_x/HZ5, which enriches the surface active oxygen and substantially enhances the catalytic activity for VC oxidation under an oxygen atmosphere.

4. Conclusions

In this study, Ce-modified ZSM-5 zeolite supported RuO_x catalysts were prepared via a two-step incipient wetness impregnation method for catalytic oxidation of VC. Experimental results reveal that cerium modification of the 1%RuO_x/HZ5 catalyst significantly enhances its activity for VC oxidation. Moreover, variations in Ce loading alter the physicochemical properties and catalytic performance of these catalysts. This phenomenon is mainly attributed to the more plentiful surface active oxygen species after Ce addition, and thereby improves the catalytic oxidation performance. Among all, 5%CeO_x-1%RuO_x/HZ5 exhibits the optimal catalytic activity. Meanwhile, the catalytic oxidation pathway of VC on the catalyst surface was analysed using *in situ* infrared spectroscopy. It is found that the Ce-modified catalyst achieves higher VC conversion efficiency and superior oxidation reactivity toward enol and carboxylic acid intermediates under an oxygen-containing atmosphere. This benefit originates from its abundant surface active oxygen species and enhanced low-temperature reducibility.

Supplementary Materials

The additional data and information can be downloaded at: https://media.sciltp.com/articles/others/2611161427126158/ESG-26090124-SI.pdf.

Author Contributions

X.Z.: Conceptualization, methodology, investigation, formal analysis, data curation, writing-original draft preparation; S.W.: Investigation, formal analysis, data curation; M.Z.: Formal analysis, data curation, validation; C.Z.: Writing—review & editing, resources, project administration, methodology, funding acquisition. All authors have read and agreed to the published version of the manuscript.

Funding

This work obtained the financial supports from Natural Science Foundation of Shandong province (ZR2025MS164) and National Natural Science Foundation of China (No. 22076088).

Institutional Review Board Statement

Not applicable.

Informed Consent Statement

Not applicable.

Data Availability Statement

Data are contained within the article and supplementary materials.

Conflicts of Interest

The authors declare no conflict of interest.

Use of AI and AI-Assisted Technologies

No AI tools were utilized for this paper.

References

1. Jia, H.; Xing, Y.; Zhang, L.; et al. Progress of catalytic oxidation of typical chlorined volatile organic compounds (CVOCs): A review. *Sci. Total Environ.* **2023**, *865*, 161063. https://doi.org/10.1016/j.scitotenv.2022.161063.
2. He, C.; Cheng, J.; Zhang, X.; et al. Recent Advances in the Catalytic Oxidation of Volatile Organic Compounds: A Review Based on Pollutant Sorts and Sources. *Chem. Rev.* **2019**, *119*, 4471–4568. https://doi.org/10.1021/acs.chemrev.8b00408.
3. Zheng, Y.; Si, W.; Zhou, B.; et al. Unveiling the Suppressive Effect of Oxygenated VOCs on Dichloromethane Catalytic Oxidation over Zeolite-Confined Ru Catalysts: Mechanism and Regulation. *Environ. Sci. Technol.* **2026**, *60*, 19693–19702. https://doi.org/10.1021/acs.est.6c04792.
4. Ding, S.; Wu, S.; Wang, P.; et al. Structure-selectivity relevance of multiple-component catalysts for CVOCs' complete oxidation: State-of-the-art and perspectives. *Sep. Purif. Technol.* **2025**, *354*, 128964. https://doi.org/10.1016/j.seppur.2024.128964.
5. Wu, S.; Hao, X.; Li, Q.; et al. Synergistic catalysis of high- and low-valence Pt sites facilitates water activation for efficient

CVOCs degradation with byproducts suppression. *Appl. Catal. B Environ. Energy* **2026**, *386*, 126371. https://doi.org/10.1016/j.apcatb.2025.126371.

6. Yan, S.; Liu, Y.; Wang, F.; et al. Breaking activity-stability tradeoff in chlorobenzene catalytic oxidation through interface construction over $SmMn_2O_5$. *J. Catal.* **2026**, *454*, 116645. https://doi.org/10.1016/j.jcat.2025.116645.
7. Xie, B.; Wang, Z.; Zhang, X.; et al. Morphology effect of cerium dioxide on the catalytic performance of Ru/CeO_2 catalyst for the oxidation of different CVOCs. *Sep. Purif. Technol.* **2024**, *345*, 127428. https://doi.org/10.1016/j.seppur.2024.127428.
8. Nie, G.; Li, R.; Bi, F.; et al. Mechanistic Insights into Potassium Poisoning of V_2O_5–MoO_3/TiO_2 Catalysts in the Synergistic Catalytic Control of NO_x and Chlorinated Organics. *ACS ES T Eng.* **2026**, *6*, 2536–2545. https://doi.org/10.1021/acsestengg.6c00430.
9. Liu, Z.; Yuan, J.; Chen, L.; et al. Crystal Phase-Dependent Opposite Catalytic Performance for Toluene and Chlorobenzene Oxidation in Simultaneous Elimination of NOx and VOCs over V_2O_5/TiO_2 Catalysts. *Environ. Sci. Technol.* **2026**, *60*, 7578–7588. https://doi.org/10.1021/acs.est.5c17618.
10. Lv, X.; Hao, X.; Xu, W.; et al. Constructing robust $Ru/CoAlO_x$ catalyst with superior lead resistance and thermal stability for chlorobenzene catalytic oxidation utilizing the anchoring effect of surface Al sites. *Appl. Catal. B Environ. Energy* **2025**, *366*, 125010. https://doi.org/10.1016/j.apcatb.2024.125010.
11. Hao, W.; Wang, Z.; Xie, S.; et al. Catalytic performance of Nb_2O_5 modified Ru/CeO_2 for dichloromethane oxidation. *Prog. Nat. Sci. Mater. Int.* **2023**, *33*, 486–494. https://doi.org/10.1016/j.pnsc.2023.08.008.
12. Wang, L.; Xu, M.; Ma, Y.; et al. Modulating electron cycling of active sites for directed chlorine species removal in dichloromethane oxidation over Ru_3CeZrO_x catalysts. *Chem. Eng. J.* **2026**, *537*, 176453. https://doi.org/10.1016/j.cej.2026.176453.
13. Wang, S.; Zhang, H.; Wang, M.; et al. Micro-meso hierarchical ZSM-5 zeolite supported RuO_x nanoparticles for activity enhancement of catalytic vinyl chloride oxidation. *Appl. Surf. Sci.* **2022**, *606*, 154906. https://doi.org/10.1016/j.apsusc.2022.154906.
14. Guo, X.; Yu, Y.; Zhang, R.; et al. Ru clusters encapsulated with Al-rich zeolite for efficiently catalytic elimination of 1,2-dichloroethane. *J. Environ. Sci.* **2026**, *159*, 10–22. https://doi.org/10.1016/j.jes.2025.02.046.
15. Liu, L.; Wu, A.; Ding, M.; et al. Facet-Dependent Interfacial Synergy in Ru/Co_3O_4 Catalysts: Manipulating Ru Speciation for Enhanced 1,2-Dichloroethane Catalytic Combustion. *ACS Catal.* **2025**, *15*, 14060–14076. https://doi.org/10.1021/acscatal.5c04183.
16. Xie, Y.; Wang, S.; Jin, P.; et al. Hierarchical ZSM-5 zeolite supported RuO_x catalysts via organic mesoporous porogens for catalytic oxidation of vinyl chloride. *Surf. Interfaces* **2024**, *45*, 103885. https://doi.org/10.1016/j.surfin.2024.103885.
17. Li, M.; Wang, Y.; Ding, M.; et al. Effect of Cu modification to Ru/HZSM-5 catalysts on the catalytic combustion of vinyl chloride. *Catal. Sci. Technol.* **2024**, *14*, 3150–3159. https://doi.org/10.1039/d4cy00300d.
18. Shen, K.; Ding, Q.; Fan, H.; et al. Biotemplate preparation of Ru/CeO_2 catalysts for the catalytic combustion of vinyl chloride. *Catal. Commun.* **2023**, *184*, 106801. https://doi.org/10.1016/j.catcom.2023.106801.
19. Sui, R.; Gao, Y.; Peng, B. Enhanced catalytic combustion of 1,2-dichloroethane over Ru_1/Al_2O_3 catalyst via regulating the Ru–O bond. *Mol. Catal.* **2026**, *593*, 115782. https://doi.org/10.1016/j.mcat.2026.115782.
20. Cao, S.; Fei, X.; Wen, Y.; et al. Bimodal mesoporous TiO_2 supported Pt, Pd and Ru catalysts and their catalytic performance and deactivation mechanism for catalytic combustion of Dichloromethane (CH_2Cl_2). *Appl. Catal. A Gen.* **2018**, *550*, 20–27. https://doi.org/10.1016/j.apcata.2017.10.006.
21. Peng, B.; Hu, Z.; Zhang, K.; et al. Synergies of redox ability and acidity over RuMn/ZSM-5 for catalytic elimination of 1,2-dichloroethane. *Sep. Purif. Technol.* **2024**, *333*, 125973. https://doi.org/10.1016/j.seppur.2023.125973.
22. Li, W.; Hu, D.; Yin, K.; et al. Hierarchical Ru-Ce/H-ZSM-5 catalysts for the catalytic oxidation of chlorobenzene: Structure-activity relationship and chlorine poisoning resistance. *Surf. Interfaces* **2022**, *34*, 102320. https://doi.org/10.1016/j.surfin.2022.102320.
23. Ying, Q.; Liu, Y.; Li, H.; et al. A comparative study of the dichloromethane catalytic combustion over ruthenium-based catalysts: Unveiling the roles of acid types in dissociative adsorption and by-products formation. *J. Colloid Interface Sci.* **2022**, *605*, 537–546. https://doi.org/10.1016/j.jcis.2021.07.095.
24. Zheng, Y.; Han, R.; Yang, Z.; et al. Engineering Subnanometric Electronic Interaction between Ru and Mn in Zeolite Boosts Catalytic Oxidation of Dichloromethane. *Environ. Sci. Technol.* **2025**, *59*, 2276–2284. https://doi.org/10.1021/acs.est.4c09264.
25. Cao, K.; Meng, Q.; Luo, X.; et al. Synergistic roles of Ru, CeO_2, and HZSM-5 in a ternary-active center catalyst for catalytic destruction of dichloromethane. *Sep. Purif. Technol.* **2024**, *339*, 126446. https://doi.org/10.1016/j.seppur.2024.126446.
26. Wang, Z.; Zhang, Q.; Shi, J.; et al. Engineering oxygen vacancies in CeO_2 for enhanced catalytic oxidation of various volatile organic compounds. *Chem. Eng. J.* **2026**, *537*, 176602. https://doi.org/10.1016/j.cej.2026.176602.
27. Gan, L.; Ye, P.; Wu, Q.; et al. Surface lattice oxygen activation and oxygen vacancies formation in Cu-doped CeO_2 for boosting catalytic oxidation of toluene. *Appl. Surf. Sci.* **2025**, *710*, 163999. https://doi.org/10.1016/j.apsusc.2025.163999.
28. Lin, H.; Lin, X.; Liu, J.; et al. Tuning surface oxygen species and defects in CeO_2-based catalysts via Ce(IV)-MOF pyrolysis for efficient toluene catalytic oxidation. *Appl. Surf.*

Sci. **2026**, *727*, 165887. https://doi.org/10.1016/j.apsusc.2026.165887.

29. Chen, X.; Wang, M.; Xu, W.; et al. Enhanced Ru dispersion via strengthened Ru-O-Ce interaction enabled by Sn-Ce solid solution for efficient chlorobenzene oxidation. *Sep. Purif. Technol.* **2025**, *379*, 134934. https://doi.org/10.1016/j.seppur.2025.134934.
30. Zhao, X.; Li, Y.; Wu, H.; et al. Catalytic activity and selectivity of Cerium-Doped catalysts in dichloromethane oxidation. *Inorg. Chem. Commun.* **2025**, *178*, 114516. https://doi.org/10.1016/j.inoche.2025.114516.
31. Gao, H.; Fan, Y.; Song, Z.; et al. Enhancing the elimination of toluene and chlorobenzene by Ce doping in α-MnO_2 to boost Lewis acidity and lattice oxygen activity. *J. Catal.* **2025**, *451*, 116346. https://doi.org/10.1016/j.jcat.2025.116346.
32. Gao, H.; Song, Z.; Mao, Y.; et al. Tight coupling of oxygen vacancies and acidity on α-MnO_2 through cerium doping engineering for efficient removal of multi-component VOCs. *Appl. Catal. B Environ. Energy* **2025**, *362*, 124745. https://doi.org/10.1016/j.apcatb.2024.124745.
33. Wu, L.; Liu, Y.; Jia, Y.; et al. A novel strategy for enhancing resistance to chlorine, water, and sulfur oxide of the Pt/Co-ZSM-5 catalyst by synergistic coupling of acidity and redox sites for the oxidation of multicomponent VOCs. *Appl. Catal. B Environ. Energy* **2025**, *378*, 125557. https://doi.org/10.1016/j.apcatb.2025.125557.
34. Ma, Z.; Fu, T.; Wang, Y.; et al. Silicalite-1 Derivational Desilication-Recrystallization to Prepare Hollow Nano-ZSM-5 and Highly Mesoporous Micro-ZSM-5 Catalyst for Methanol to Hydrocarbons. *Ind. Eng. Chem. Res.* **2019**, *58*, 2146–2158. https://doi.org/10.1021/acs.iecr.8b03858.
35. Ruan, Y.; Liu, P.; Liu, J.; et al. Dual Regulation of Oxygen Vacancies and Metal–Support Interaction in Ni/NixCeO_2-γ for Synergistic Enhancement of Low-Temperature CO_2 Methanation. *ACS Catal.* **2026**. https://doi.org/10.1021/acscatal.6c03681.
36. Xu, J.; Li, H.; Song, J.; et al. Orbital-Engineered Sn/RuO_2 Nanocatalyst with Self-Regulating Electron Configuration for Durable Chlorine Evolution at Industrial Current Densities. *ACS Appl. Mater. Interfaces* **2026**, *18*, 38800–38814. https://doi.org/10.1021/acsami.6c08004.
37. Xu, X.; Ling, Y.; Bi, J.; et al. Rational Design of Ru-CeO_2/Al_2O_3 Composite Catalysts: Insight into Special Catalytic Behavior in Dimethyl Disulfide Oxidation. *Ind. Eng. Chem. Res.* **2026**, *65*, 3622–3633. https://doi.org/10.1021/acs.iecr.5c04383.
38. Ding, M.; Wang, Y.; Li, M.; et al. Sulfur-Engineered Ru/SnO_2 Catalysts for Highly Efficient Catalytic Combustion of 1,2-Dichloroethane. *Environ. Sci. Technol.* **2025**, *59*, 15445–15456. https://doi.org/10.1021/acs.est.5c03212.
39. Khalid, O.; Spriewald Luciano, A.; Drazic, G.; et al. Mixed $Ru_xIr_{1-x}O_2$ Supported on Rutile TiO_2: Catalytic Methane Combustion, a Model Study. *ChemCatChem* **2021**, *13*, 3983–3994. https://doi.org/10.1002/cctc.202100858.
40. Xing, X.; Wang, Y.; Wu, B.; et al. Catalytic Co-Oxidation of Acetone and Ammonia over Metal–Organic Framework-Derived Ce–Cu Oxides: Structure–Activity Relationship and Pollutant Interaction Mechanism. *Langmuir* **2026**, *42*, 24664–24681. https://doi.org/10.1021/acs.langmuir.6c03941.
41. Ma, S.; Dong, F.; Wu, S.; et al. Constructing a Stable Single-Atom Pt Catalyst on CeO_2 Nano-Islands to Enhance Water Resistance and Catalysis Performance via H_2O Activation. *ACS Appl. Mater. Interfaces* **2026**, *18*, 42712–42725. https://doi.org/10.1021/acsami.6c11200.
42. Su, J.; Xie, S.; Shen, Y.; et al. Structure-Performance Relationship of Morphology-Dependent CeO_2 Catalysts in Toluene Oxidation. *Inorg. Chem.* **2026**, *65*, 14097–14111. https://doi.org/10.1021/acs.inorgchem.6c01534.
43. Xu, Z.; Feng, Y.; Yang, X.; et al. Engineering Inverse CuO@CeO_2 Interfaces with Tandem Active Sites to Boost Low-Temperature Catalytic Degradation of Malodorous Methyl Mercaptan. *Environ. Sci. Technol.* **2026**, *60*, 20660–20676. https://doi.org/10.1021/acs.est.6c01807.
44. Zhang, X.; Dai, L.; Liu, Y.; et al. Effect of support nature on catalytic activity of the bimetallic RuCo nanoparticles for the oxidative removal of 1,2-dichloroethane. *Appl. Catal. B Environ.* **2021**, *285*, 119804. https://doi.org/10.1016/j.apcatb.2020.119804.
45. Yu, X.; Dai, L.; Deng, J.; et al. An isotopic strategy to investigate the role of water vapor in the oxidation of 1,2-dichloroethane over the Ru/WO_3 or Ru/TiO_2 catalyst. *Appl. Catal. B Environ.* **2022**, *305*, 121037. https://doi.org/10.1016/j.apcatb.2021.121037.
46. Zhang, H.; Wang, S.; Wang, M.; et al. Catalytic oxidation of vinyl chloride over Co–Ce composite oxides derived from ZIF-67 template: Effect of cerium incorporation. *J. Rare Earths* **2023**, *41*, 870–880. https://doi.org/10.1016/j.jre.2022.12.006.
47. Zhang, H.; Cao, H.; Li, G.; et al. Oxygen vacancy engineering by La-incorporation into Co_3O_4 matrix for boosting catalytic oxidation of vinyl chloride: Experimental and DFT evidences. *J. Catal.* **2026**, *453*, 116524. https://doi.org/10.1016/j.jcat.2025.116524.
48. Deng, Z.; Wang, S.; Li, G.; et al. Mn-Zr composite oxides for catalytic vinyl chloride oxidation: The deactivation and mechanism study. *Inorg. Chem. Commun.* **2023**, *152*, 110647. https://doi.org/10.1016/j.inoche.2023.110647.